# A Static Core-Edge Simulation of *H*-mode Tokamak Plasmas using BALDUR and TASK/TR Codes

N. Poolyarat 1), Y.Pianroj 2), T.Onjun 2), A. Fukuyama 3), S. Suwanna 2), and R. Picha 4)

1) Department of Physics, Thammasat University, Pathumthani, Thailand.
2) School of Manufacturing and Mechanical Engineering, Sirindhorn International Institute of Technology, Thammasat University, Pathumthani, Thailand.
3) Department of Nuclear Engineering, Kyoto University, Kyoto, Japan.
4) Thailand Institute of Nuclear Technology, Bangkok, Thailand.
E-mail contact of main author: nop096@tu.ac.th

**Abstract**. A theory-based model for self-consistently predicting a pedestal formation of temperature and density is developed and employed together with a core transport model either in 1.5D BALDUR or TASK/TR integrated predictive modelling codes for simulating *H*-mode tokamak plasmas. In the core plasma, an anomalous transport is computed using a semi-empirical Mixed Bohm/gyro-Bohm (Mixed B/gB), while a neoclassical transport is computed using the NCLASS model. For the pedestal, electron and ion thermal, particle and impurity transports are separately suppressed by $\omega_{E\times B}$ flow shear and magnetic shear. Because of the reduction of anomalous transport, the formation of pedestal can be developed. This core-edge model is used to simulate the time evolution of plasma current, temperature, and density profiles for DIII-D tokamaks. It is found that the pedestal can be self-consistently formed in both BALDUR and TASK/TR simulations. A statistical analysis is also carried out to quantify the agreement with the experimental data. It is found that the simulation results that carried out by BALDUR show an agreement for core-edge model with %RMSE less than 21% and 18% for temperature profiles and density profiles, respectively and TASK/TR code shows %RMSE less than 20% and 10% for temperature profiles and density profiles, respectively.

## 1. Introduction

A major advance in magnetic confinement fusion occurred with the discovery of a new operating regime, called the "High confinement mode" (*H*-mode) [1]. The *H*-mode operation results in a significant increase in the plasma temperature and confinement time. The large increase is the result of a transport barrier that is formed at the edge of the *H*-mode plasma. This edge transport barrier (ETB) is usually referred as the "pedestal". Typically, the energy content in an *H*-mode discharge is approximately twice the energy contained in an *L*-mode discharge, for the plasma heated with the same input power [2].

To develop a better understanding of the physical processes and the interrelationships between those physical processes that occurs in tokamak plasma experiments, advanced computer codes are developed to improve understanding of plasma behaviours. The integrated predictive modelling codes, such as BALDUR [3], TASK/TR [4], JETTO [5], ASTRA [6] and CRONOS [7], have played an important role in carrying out simulations in order to predict the time evolution of plasma current, temperature, and density profiles. Many of the simulations carried out with these integrated predictive modelling codes make use of boundary conditions taken from experimental data. In simulating *H*-mode discharge, the evolution of the core plasma was carried out using boundary conditions taken from experimental data at the top of the pedestal [8-13]. The distance from the top of the pedestal to the center of plasma is approximately 95% of the total radius. Several years after discovery of the *H*-mode scenario, however, researchers found different physical phenomena at the plasma edge area such as the formation of pedestal that have effects on the plasma core area. The pedestal formation requires a reduction of fluctuation-driven transport, which can be achieved by stabilization or decorrelation of microturbulence in the plasma. The stabilization mechanisms, which can suppress turbulent modes, have to account for the different dynamical behaviors of the various species in the plasma. The first candidate for edge turbulence

stabilization is the $\omega_{E\times B}$ flow shear. The $\omega_{E\times B}$ flow shear can suppress turbulence by linear stabilization of turbulent modes, and in particular by non-linear decorrelation of turbulence vortices [14-16], thereby reducing transport by acting on both the amplitude of the fluctuations and the phase between them [17]. The second candidate is additional magnetic shear stabilization (*s*), which is reduced only in the region where the magnetic shear *s* exceeds the threshold and is unaffected elsewhere; more details will be provided in section 3.

## 2. Modeling of core plasma

The Mixed Bohm/gyro-Bohm (B/gB) core transport model [18] is an empirical transport model. It was originally a local transport model with Bohm scaling. A transport model is said to be "local" when the transport fluxes (such as heat and particle fluxes) depend entirely on local plasma properties (such as temperatures, densities, and their gradients). Mixed B/gB transport model can be expressed as follows[19]:

$$\chi_e = 1.0\chi_{gB} + 2.0\chi_B \tag{1}$$

$$\chi_i = 0.5\chi_{gB} + 4.0\chi_B + \chi_{neo} \tag{2}$$

$$D_H = [0.3 + 0.7\rho]\frac{\chi_e\chi_i}{\chi_e+\chi_i} \tag{3}$$

$$D_z = D_H \tag{4}$$

where,

$$\chi_{gB} = 5\times 10^{-6}\sqrt{T_e}\left|\frac{\nabla T_e}{B_\phi^2}\right| \tag{5}$$

$$\chi_B = 4\times 10^{-5}R\left|\frac{\nabla(n_eT_e)}{n_eB_\phi}\right| q^2\left(\frac{T_{e,0.8}-T_{e,1.0}}{T_{e,1.0}}\right)\times\Theta\left(-0.14+s-\frac{1.47\omega_{E\times B}}{\gamma_{ITG}}\right) \tag{6}$$

where, $\chi_e$ is the electron diffusivity, $\chi_i$ is the ion diffusivity, $D_H$ is the particle diffusivity, $D_z$ is the impurity diffusivity, $\chi_{gB}$ is the gyro-Bohm contribution, $\chi_B$ is Bohm contribution, $\rho$ is normalized minor radius, $T_e$ is the electron temperature in keV, $B_\phi$ is the toroidal magnetic field (T), $R$ is the major radius (m), $n_e$ is the local electron density, $q$ is the safety factor, $s$ is the magnetic shear, $\omega_{E\times B}$ is the flow shearing rate, and $\gamma_{ITG}$ is the ion temperature gradient (ITG) growth rate, estimated as $v_{ti}/qR$ [20], in which $v_{ti}$ is the ion thermal velocity. The $\Theta$-function is the Heaviside step function that it is the empirical ITB formation threshold condition that was found in [20].

## 3. Modeling of Edge Plasma

The major purpose of modelling the edge transport is to understand and predict the formation of the pedestal structure such as the variation of the pedestal widths and heights of the plasma density and temperature. The modelling of the transport barrier width is not yet well developed. An appropriate transport suppression function ($f_s$) due to $\omega_{E\times B}$ flow shearing rate together with the reduction of turbulence growth rate [21-23] is represented in the first term which the $E\times B$ flow shear alone produces pedestals which are appreciably lower than those experimentally obtained. Therefore, an additional magnetic shear stabilization ($s$) is

supposed in the second term [24, 25]. The transport is reduced only in the region where the magnetic shear exceeds the threshold (in this work the threshold equals to 0.5 [25]) and the suppression function can be shown in Eq.(7). Moreover, we assume all the simulations evolved the temperature pedestal width and height during the ELM-free phase.

$$f_{s_x} = \frac{1}{1+C_x\left(\frac{\omega_{E\times B}}{\gamma_{ITG}}\right)^2} \times \frac{1}{\max\left(1,(s-0.5)^2\right)} \tag{7}$$

where, $C_x$ is the coefficient for each species that is shown in Table 1.

**Table1:** The coefficient for each species that used in this work.

| Codes | $C_i$ | $C_e$ | $C_H$ | $C_z$ |
|---|---|---|---|---|
| BALDUR | $4.50\times 10^3$ | $4.50\times 10^3$ | $1.00\times 10^2$ | $1.02\times 10^2$ |
| TASK/TR | $1.00\times 10^0$ | $1.00\times 10^0$ | $1.00\times 10^0$ | $1.00\times 10^0$ |

Note that the coefficients in BALDUR are greater than TASK/TR, because the density profiles obtain in the different method; BALDUR used a predicted density profile, but TASK/TR used a fixed density profile. Therefore, by using the suppression function suppressed every channel of transports. The suppression of ion thermal diffusivity ($\chi_{i_s}$), suppression of electron thermal diffusivity ($\chi_{e_s}$), suppression of hydrogenic particle diffusivity ($D_{H_s}$) and suppression of impurity particle diffusivity ($D_{z_s}$) are given by Eq.(8-11).

$$\chi_{i_s} = \chi_i \times f_{s_{ion}} \tag{8}$$
$$\chi_{e_s} = \chi_e \times f_{s_{eletron}} \tag{9}$$
$$D_{H_s} = D_H \times f_{s_{Hydrgenic}} \tag{10}$$
$$D_{z_s} = D_z \times f_{s_{impurity}} \tag{11}$$

## 4. Simulation results and discussions

### 4.1. Simulated Plasma Profiles

All the experimental data from 10 DIII-D *H*-mode discharges considered in this paper are taken from the international profile data base [26] and major plasma parameters for all of ten discharges are listed in Table 2.

**Table 2**: Details of plasma parameters from each discharge.

| Discharges | 77557 | 77559 | 81321 | 81329 | 81499 | 81507 | 82205 | 82788 | 82188 | 82183 |
|---|---|---|---|---|---|---|---|---|---|---|
| Type | Low power | High power | Low $n_e$ | High $n_e$ | Low $\kappa$ | High $\kappa$ | Low $\rho^*$ | High $\rho^*$ | - | - |
| $R$(m) | 1.68 | 1.69 | 1.69 | 1.70 | 1.69 | 1.61 | 1.69 | 1.68 | 1.69 | 1.69 |
| $a$(m) | 0.62 | 0.62 | 0.60 | 0.59 | 0.63 | 0.54 | 0.63 | 0.62 | 0.63 | 0.54 |
| $\kappa$ | 1.85 | 1.84 | 1.83 | 1.83 | 1.68 | 1.95 | 1.71 | 1.67 | 1.65 | 1.91 |
| $\delta$ | 0.33 | 0.35 | 0.29 | 0.36 | 0.32 | 0.29 | 0.37 | 0.35 | 0.29 | 0.22 |
| $B_T$(T) | 1.99 | 1.99 | 1.98 | 1.94 | 1.91 | 1.91 | 1.87 | 0.94 | 1.57 | 1.57 |
| $I_p$(MA) | 1.00 | 1.00 | 1.00 | 1.00 | 1.35 | 1.34 | 1.34 | 0.66 | 1.33 | 1.33 |
| $\overline{n_e}(10^{19}m^{-3})$ | 4.88 | 5.02 | 2.94 | 5.35 | 4.81 | 4.90 | 5.34 | 2.86 | 6.47 | 6.87 |
| $Z_{eff}$ | 1.68 | 2.21 | 2.42 | 1.65 | 2.33 | 1.93 | 2.13 | 1.94 | 1.95 | 1.95 |
| $P_{NB}$(MW) | 4.78 | 13.23 | 3.49 | 8.34 | 5.74 | 5.71 | 5.86 | 3.25 | 3.92 | 3.92 |
| Diagnostic time (s) | 2.70 | 2.70 | 3.90 | 3.80 | 4.00 | 3.80 | 3.66 | 3.54 | 3.78 | 3.78 |

In these simulations, there are two types of simulations: the core simulations are calculated using experimental boundary and the core-edge simulations are calculated with a pedestal model included 10-eV temperature and $1 \times 10^{17} m^{-3}$ density at seperatrix. It should be noted that the change of edge temperature does not affect the simulation results. In Fig.1, the profiles of electron temperature, ion temperature, electron density and deuterium density as functions of minor radius are carried out by BALDUR and TASK/TR for DIII-D discharge 82205 and 81329 at the diagnostic time. The shapes of all profiles remained nearly the same in the discharges of experimental data and show good agreement with the experiment data when evaluated by using the statistical analysis. More details will be discussed in the next section. Unfortunately, there are no results for impurity in the database for these DIII-D discharges.

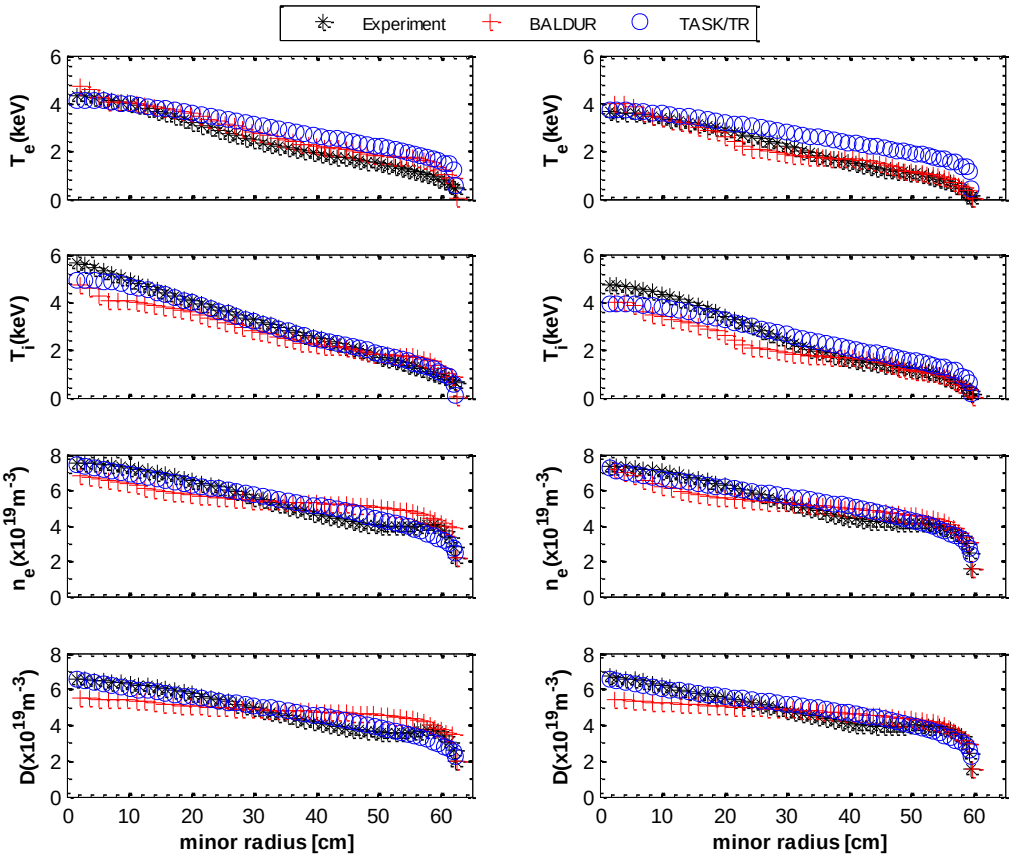


**FIG.1**: The profiles of electron temperature, ion temperature electron density and deuterium density as a function of minor radius. The simulation results are carried out by BALDUR and TASK/TR with core-edge transport model compared to the DIII-D experimental data discharge 82205(left panel) and 81329 (right panel) at the diagnostic time.

The mechanism that helps to stabilize the anomalous transport and to form the transport barrier at the plasma edge is described by the suppression function that was shown in Eq.7 and Fig.2. This function is composed of two terms which suppress the turbulent transport. The first term is $E \times B$ flow shear, which likely plays a role to reduce the turbulent transport. In this work, it acts at normalized minor radius (r/a) = 0.9-1.0. The effect of $E \times B$ flow shear stabilization is considered to be important in allowing transport barrier formation. To demonstrate this effect appropriately the radial electric field ($E_r$) carried out by BALDUR and TASK/TR are shown in this figure. Both profiles of $E_r$ have similar shape and show greater strength near the edge area (at minor radius 58 cm); however, the absolute magnitude of the

radial electric field carried out by TASK/TR is higher than $E_r$ that carried out by BALDUR, thus the radial electric field will affect the $\omega_{E\times B}$ flow shear [27] that is depicted below.

$$\omega_{E\times B} = \frac{(RB_\theta)^2}{B_\emptyset}\left(\frac{\partial}{\partial\psi}\right)\frac{E_r}{RB_\theta} \tag{12}$$

where, $R$ is the major radius, $B_\theta$ is the poloidal magnetic field and $B_\emptyset$ is the toroidal magnetic field. The $\omega_{E\times B}$ flow shear calculated by the predictive modelling codes is shown in Fig.2, and shows the same trend as the radial electric field pattern where the magnitude is very strong at the plasma edge. The last term, the magnetic shear, also plays a key role in facilitating entry into enhanced confinement or low magnetic shear acts to reduce turbulence growth rates [28, 29]. Thus, the magnetic shear profiles simulated by BALDUR and TASK/TR are shown in this figure. The magnetic shear increases swiftly at r/a = 0.6-1.0, therefore the inverse of maximum function between 1 to $(s-0.5)^2$ of this term works to suppress the transport at the plasma edge area, too. The trends of these parameters carried out by BALDUR and TASK/TR are quite similar, as explained above in every ten DIII-D discharges which were used in this work.

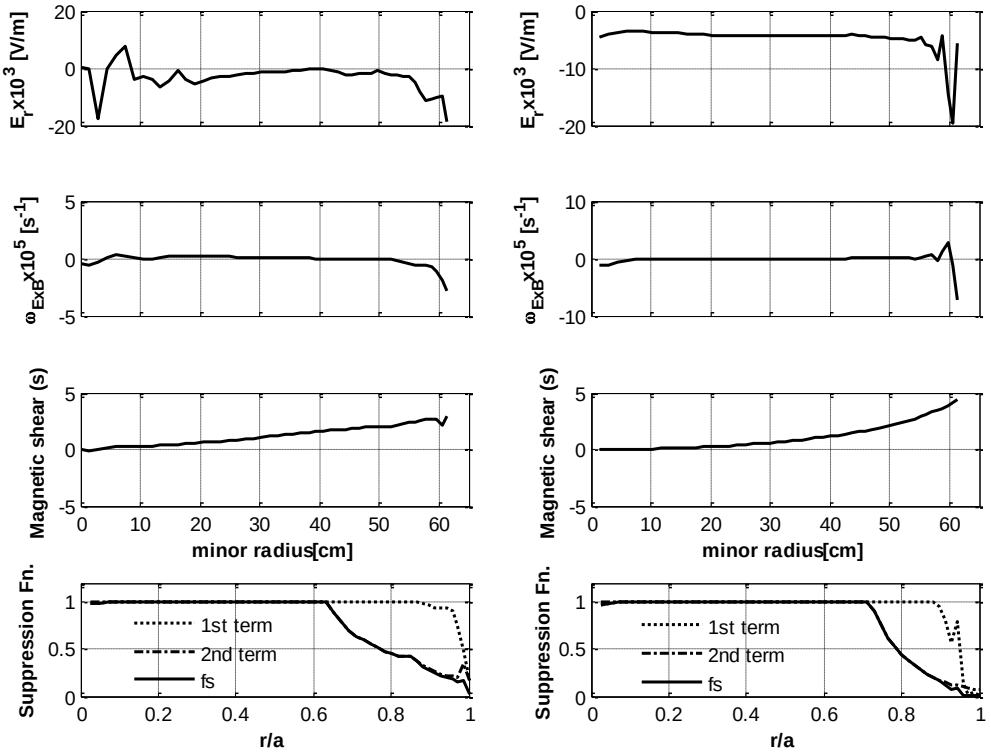


**Fig 2**: The radial electric field, $\omega_{E\times B}$ flow shear, magnetic shear as a function of minor radius and the suppression function as the normalized minor radius carried out by the predictive modelling codes BALDUR (left panel) and TASK/TR (right panel) of DIII-D device discharge 82205 at simulation time 3.025 sec.

### 4.2 Statistical analysis

To quantify the comparison between simulations and experimental data, the percentage of the root-mean-square error (%RMSE) deviation and the %offset are computed based on the difference between simulation results and experimental data. In this paper, the %RMSE and the %offset are defined as Eq. (13) and (14), respectively.

$$\%\text{RMSE} = \sqrt{\frac{1}{N}\sum_{i=1}^{N}\left(\frac{X_{exp_i} - X_{sim_i}}{X_{exp_0}}\right)^2} \times 100 \quad (13)$$

$$\%\text{offset} = \frac{1}{N}\sum_{i=1}^{N}\left(\frac{X_{exp_i} - X_{sim_i}}{X_{exp_0}}\right) \times 100 \quad (14)$$

where, $X_{exp_i}$ is the $i$th data point of the experimental profile, $X_{sim_i}$ is the corresponding data point of the simulation profile, and $X_{exp_0}$ is the maximum data point of the experimental profile of $X$ as a function of radius, which has $N$ points in total. The %RMSE and the %offset are evaluated for each of the four profiles: electron temperature, ion temperature, electron density and deuterium density for the discharges considered. Note that the %offset is positive if the simulated profile is higher than the experimental profile and negative if the simulated profile is lower than the experimental profile. If the %offset is zero, then the %RSME is a measure of how much the shape of the profiles differs between simulated and experimental.

### 4.2.1 Simulation results compared with 10 DIII-D *H*-mode discharges

In this section, the simulation results carried out by BALDUR and TASK/TR codes are validated with 10 DIII-D experimental data by using the statistical analysis. It should be noted that the statistical analysis in this work consists of two groups. The first group is named “core model” which is used to quantify all the simulation and experimental data when the simulation data are calculated by using anomalous transport Mixed B/gB from the center of plasma to the top pedestal in which the boundary is taken from experiments at the top of pedestal at the diagnostic time. Another group is named “core-edge model” which is used to quantify all the simulation and experimental data when the simulation data are calculated by using the anomalous transport Mixed B/gB which included suppression function from the center to the edge of plasma (separatrix). The average of %RMSE (%$\text{RMSE}_{avg}$) and average of %offset (%$\text{offset}_{avg}$) averaged over 10 discharges for electron temperature, ion temperature, electron density and deuterium density. All the details of the analysis are shown in Fig.3. They show the difference of the %$\text{RMSE}_{avg}$ of thermal channels (both electron and ion) increasing 7% for BALDUR and 6% for TASK/TR, after core-edge model has implemented in these codes and for density channel in BALDUR, the %$\text{RMSE}_{avg}$ decrease 5% in case of electron density and increase 1% in case of deuterium density; however, for density channel in TASK/TR, the %$\text{RMSE}_{avg}$ for both electron and deuterium densities are the same value because the TASK/TR code used the fixed density profiles which were taken from the DIII-D experimental data.

In cases of %$\text{offset}_{avg}$, after implemented the core-edge model in the BALDUR code. It found that the %$\text{offset}_{avg}$ of electron temperature shows lower prediction when compared the simulation results with the experimental results as well as the %$\text{offset}_{avg}$ of electron temperature in the TASK/TR code shows mostly negative that means the code underpredicts the experimental data. The %$\text{offset}_{avg}$ of ion temperature that predicted from both codes shows the same trend. It is increased mostly positive after the core-edge was implemented. It can be indicated that simulation overpredict the experimental data. Moreover, the %$\text{offset}_{avg}$ of electron density that predicted from BALDUR code with core-edge model shows overpredict but the yield of %$\text{offset}_{avg}$ is decreased 7%, indicating that simulations approach to experimental data due to the %$\text{RMSE}_{avg}$ reduced, too and the %$\text{offset}_{avg}$ of deuterium density that predicted from BALDUR code with core-edge model shows quite underpredict. As

mention above, the density profiles from TASK/TR code are fixed that reason why the $\%offset_{avg}$ of electron and deuterium density do not change anything.

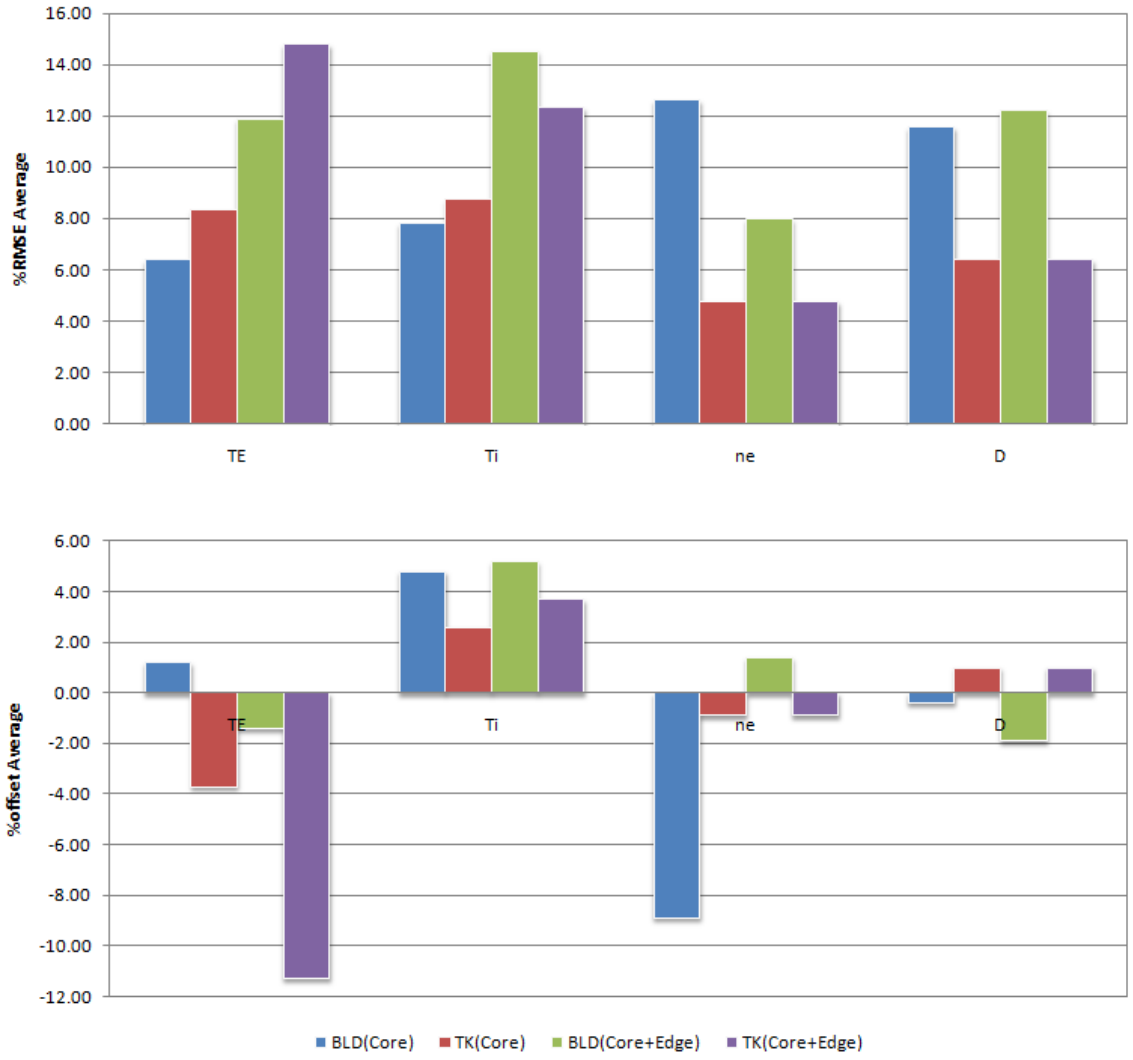


**Fig 3**: The average percentage of root mean square error ($\%RMSE_{avg}$) and the average percentage of offset ($\%offset_{avg}$) for all four profiles: electron temperature ($T_e$), ion temperature ($T_i$), electron density ($n_e$) and deuterium density (D) produced by simulations using the core and core-edge models compared with experimental data for the 10 *H*-mode discharges listed in Table 2.

## 5. Conclusions

The core simulations carried out using BALDUR and TASK/TR codes with Mixed B/gB core model and prescribed boundary conditions yield a fairly satisfactory prediction capability BALDUR code yields less than 12 and 26 %RMSE for temperature and density profiles, respectively. TASK/TR code produces less than 16 and 10 %RMSE for quantities. After the core-edge model has been implemented into the integrated predictive modelling codes, it gives good results with %RMSE less than 21% and 18% for BALDUR, and 20% and 10% for TASK/TR, for temperature profiles and density profiles, respectively.

**Acknowledgments** This work is supported by the Commission on Higher Education (CHE) and the Thailand Research Fund (TRF) under Contract No RMU5180017 and the Commission on Higher Education, Thailand for supporting by granting fund under the program "Strategic Scholarships for Frontier Research Network for the Ph.D. Program Thai Doctoral Degree", and partially supported by Grant-in-Aid for Scientific Research (S) (20226017) from JSPS, Japan. The authors would also thank Thammasat University research fund for travel grant to present this work.

**References:**

[1] Wagner F. *et al* 1982 *Phys. Rev. Lett.* **49(19)** 1408
[2] Connor J. W. and Wilson H. R. 2000 *Plasma Phys. Control. Fusion* **42** R1-R74
[3] Singer C. E. *et al* 1988 *Comput. Phys. Commun.* **49** 275-398
[4] Honda M. and Fukuyama A. 2006 *Nuclear Fusion* **46** 580-593
[5] Cenacchi G. and Taroni A. 1988 *JET-IR* **88**
[6] Pereverzev G. and Yushmanov P. N. 2002 *Max-Planck Institut fur Plasmaphysik* **IPP 5/98**
[7] Basiuk V. *et al* 2003 *Nuclear Fusion* **43** 822
[8] Kinsey J. E. *et al* 2002 *Phys. Plasmas* **9(5)** 1676
[9] Bateman G. *et al* 1998 *Physics of Plasmas* **5** 1793
[10] Bateman G. *et al* 2003 *Plasma Phys. Control. Fusion* **45** (11) 1939-1960
[11] Kinsey J. E. *et al* 2003 *Nuclear Fusion* **43** (12) 1845
[12] Onjun T. *et al* 2001 *Phys. Plasmas* **8** 975
[13] Hannum D. *et al* 2001 *Phys. Plasmas* **8** 964
[14] Biglari H. *et al* 1990 *Physics of Fluids B: Plasma Physics* **2** (1) 1-4
[15] Gohil P. 2006 *Comptes Rendus Physique* **7** (6) 606-621
[16] Boedo J. *et al* 2000 *Nucl. Fusion* **40** 1397
[17] Oost G. V. *et al* 2003 *Plasma Phys. Control. Fusion* **45** 1-23
[18] Tala T. J. J. *et al* 2001 *Plasma Phys. Control. Fusion* **43** 507
[19] Onjun T. and Pianroj Y. 2009 *Nuclear Fusion* **49** 075003
[20] Tala T., Helsinki University of Technology, 2002.
[21] Zolotukhin O. V. *et al*, in *28th EPS Confer. on Contr. Fusion and Plasma Phys.* (Funchal, Portugal, 2001), Vol. 25A, pp. 677-680.
[22] Sugihara M. *et al*, in *28th EPS Conf. on Contr. Fusion and Plasma Phys.* (Funchal, Portugal, 2001), Vol. 25A, pp. 629-632.
[23] Pankin A. Y. *et al* 2005 *Plasma Physics and Controlled Fusion* (3) 483
[24] Janeschitz G. and et al. 2002 *Plasma Physics and Controlled Fusion* **44** (5A) A459
[25] Pacher G. W. and et al. 2004 *Plasma Physics and Controlled Fusion* **46** (5A) A257
[26] Boucher D. *et al* 2000 *Nuclear Fusion* **40** (12) 1955
[27] Burrell K. H. 1997 *Phys. Plasmas* **4** 1499
[28] Doyle E. J. *et al* 2007 *Nuclear Fusion* **47** (6) S18
[29] Waltz R. E. *et al* 1997 *Phys. Plasmas* **4** (7) 2482